Research article

A conserved arginine with non-conserved function is a key determinant of agonist selectivity in α7 nicotinic acetylcholine receptors

Teresa Minguez-Viñas[a], Beatriz E. Nielsen[b], Deborah K. Shoemark[c], Cecilia Gotti[d], Richard B. Sessions[c], Adrian J. Mulholland[e], Cecilia Bouzat[b], Susan Wonnacott[f], Timothy Gallagher[e], Isabel Bermudez[a][1], A Sofia Oliveira[c][e][2]

[a]Department of Biological and Medical Sciences, Oxford Brookes University, Oxford OX3 0BP (United Kingdom); [b]Instituto de Investigaciones Bioquímicas de Bahía Blanca, Departamento de Biología, Bioquímica y Farmacia, Universidad Nacional del Sur-Consejo Nacional de Investigaciones Científicas y Técnicas (CONICET), Bahía Blanca 8000 (Argentina); [c]School of Biochemistry, University of Bristol, Bristol BS8 1DT (United Kingdom); [d]CNR, Institute of Neuroscience, Biometra Department, University of Milan, I-20129 Milan (Italy); [e]School of Chemistry, University of Bristol, Bristol BS8 1TS (United Kingdom); [f]Department of Biology and Biochemistry, University of Bath, Bath BA2 7AY (United Kingdom).

Short Title: A β3-strand arginine is a subtype selectivity element in nAChR

Corresponding authors:

      * Isabel Bermudez   * A Sofia Oliveira

Email: ibermudez@brookes.ac.uk   sofia.oliveira@bristol.ac.uk

Keywords: Nicotinic acetylcholine receptors, agonist selectivity, cytisine, C(10) cytisine derivatives.

Data availability statement

The data that support the findings of this study are available from the corresponding author upon reasonable request. Some data may not be made available because of privacy or ethical restrictions.

ABSTRACT

BACKGROUND AND PURPOSE:

The $\alpha7$ and $\alpha4\beta2*$ (* denotes possibly assembly with another subunit) nicotinic acetylcholine receptors (nAChR) are the most abundant nAChR in the mammalian brain. These receptors are also the most commonly targeted nAChR in drug discovery programs for brain disorders. However, the development of subtype-specific agonists remains challenging, mainly due to the high degree of sequence homology and conservation of function in nAChR. We have developed C(10) variants of cytisine, a partial agonist of $\alpha4\beta2$ nAChR that has been used for smoking cessation. The C(10) methyl analogue used in this study displays negligible affinity for $\alpha7$ nAChR, while retaining high-affinity for $\alpha4\beta2$ nAChR.

EXPERIMENTAL APPROACH:

The structural underpinning of the selectivity of 10-methylcytisine for $\alpha7$ and $\alpha4\beta2$ nAChR was investigated using molecular dynamics simulations, mutagenesis and whole-cell and single-channel current recordings.

KEY RESULTS:

We identified a conserved arginine in the $\beta3$-strand that exhibits a non-conserved function in nAChR. In $\alpha4\beta2$ nAChR, the arginine forms a salt-bridge with an aspartate residue in loop B that is necessary for receptor expression, whereas in $\alpha7$ nAChR, this residue is not stabilised by electrostatic interactions, making its side chain highly mobile. This lack of constrain produces steric clashes with agonists and affects the dynamics of residues involved in agonist binding and the coupling network.

CONCLUSIONS AND IMPLICATIONS:

We conclude that the high mobility of the $\beta3$-strand arginine in the $\alpha7$ nAChR influences agonist binding, and possibly gating network and desensitisation. The findings have implications for rational design of subtype-selective nAChR agents.

ABBREVIATIONS

Bungarotoxin, Bgtx; extracellular domain, ECD; nicotinic acetylcholine receptor, nAChR; cytisine, Cyt; 10-methylcytisine, MeCyt; principal component analysis, PCA; root mean square deviation, RMSD; root mean square fluctuation, RMSF.

Bullet point summary:

What is already known?

- The primary target for current smoking cessation drugs such as cytisine is the α4β2 nAChR.

- The broad nAChR selectivity of cytisine, which includes α7nAChR, may contribute to off-target effects.

What this study adds?

- An arginine in β3-strand in α7 nAChR modulates binding of cytisine and 10-methylcytisine to α7 nAChR.

- The equivalent arginine residue in α4β2 nAChR has no impact on agonist selectivity or receptor function but is necessary for receptor expression.

What is the clinical significance?

- The β3-strand arginine may be useful for developing α4β2-targeted drugs with no activity in α7 nAChR.

1 INTRODUCTION

Nicotinic acetylcholine receptors (nAChR) are a major branch of the Cys loop neurotransmitter-gated ion channel family, which also includes the $GABA_A$, glycine and $5\text{-}HT_3$ receptors (Corringer et al., 2000). The most prevalent nAChR in the mammalian brain are the $\alpha4\beta2^*$ (* denotes possibly assembly with another subunit) and α7 subtypes (Gotti et al., 2009). These subtypes are the most commonly targeted nAChR in drug discovery programs for neurological and neuropsychiatric disorders (Dineley et al., 2015). Additionally, $\alpha4\beta2^*$ nAChR play a central role in mediating the rewarding and reinforcing actions of nicotine (Maskos et al., 2005). Consequently, partial agonists of $\alpha7$ and $\alpha4\beta2^*$ nAChR are established targets to modulate the function of these subtypes in brain disorders and for aiding smoking cessation (Hogg and Bertrand, 2007; Coe et al., 2009). However, the development of agonist specific $\alpha7$ or $\alpha4\beta2$ remains challenging due to the structural similarity between nAChR subtypes (Corringer et al., 2000) (Figure S1A), and currently only the smoking cessation drugs varenicline (Champix®/Chantix®) and cytisine (Tabex®) are available clinically. Despite the proven efficacy of varenicline (Hajek et al., 2013b) and cytisine (Hajek et al., 2013a) off-target effects continue to be problematic (Tonstad et al., 2010; Hajek et al., 2013b, 2013a). This is likely due to the ability of these compounds to activate most nAChR subtypes, including the $\alpha7$ nAChR, at which they display full agonism, albeit with much-reduced binding and functional affinity than at $\alpha4\beta2^*$ nAChR, their intended target (Rego-Campello et al., 2018). Consequently, there is interest in identifying structural elements associated with agonist specificity that differ between the $\alpha4\beta2$ and $\alpha7$ nAChR.

Our work in this area has focused on developing cytisine analogues functionalised at position C(10) of the pyridone moiety (Figure 1A). These C(10) substituents are predicted to occupy a region in the agonist pocket between the complementary subunit and loop C of the principal subunit, enabling interactions with residues from both regions (Figure S1B) (Rego-Campello et al., 2018). Although we have found that the C(10) cytisine variants share the same core-binding interactions as cytisine in the $\alpha7$ and $\alpha4\beta2$ nAChR (Figure S1B), these compounds display negligible affinity for the $\alpha7$ subtype, while retaining selectivity for $\alpha4\beta2$ nAChR (Rego-Campello et al., 2018). A recent study using unnatural amino acid chain substitutions to probe the binding interactions of cytisine and its C(10) variants in the $\alpha4\beta2$ nAChR, showed that these substitutions only have a modest effect on interactions with residues in loop C and E, depending on the C(10) substituent's steric bulk or electronic properties (Blom et al., 2019); however, the conservation of these residues in $\alpha7$ nAChR fails to explain the selectivity of the C(10) variants of cytisine.

To identify the structural elements underpinning the receptor selectivity of C(10)-substituted cytisine variants, we have compared the dynamical behaviour of α7 and α4β2 nAChR bound to ACh, (-)-cytisine or its (-)-C(10)-methyl variant, 10-methylcytisine (Figure 1A). Here, we identify a conserved arginine residue in β3-strand that in α7 nAChR not only orchestrates the suppression of agonism for 10-methylcytisine but also modulates agonist binding and channel function. In the α4β2 subtype, the analogous arginine mainly affects receptor expression. Our results have implications for the rational design of subtype-specific nAChR ligands.

2 METHODS

2.1 Materials

Varenicline and (-)-cytisine were purchased from Tocris, UK. (-)-10-methylcytisine was synthesized (and provided as the HCl salt) at the School of Chemistry, University of Bristol (Rego-Campello et al., 2018). (±)-[^{3}H]epibatidine (specific activity of 56-60 Ci/mmol) and [^{125}I]Bungarotoxin ([^{125}I]Bgtx) (specific activity 200-213 Ci/mmol) were purchased from PerkinElmer, Boston MA. (±)Epibatidine, unlabeled bungarotoxin and collagenase Type 1A were obtained from Sigma-Aldrich, UK.

2.2 Animals

Xenopus laevis toads were housed and cared for following the UK Home Office code of practice guidelines for the species. The collecting of oocytes from *Xenopus* toads was carried in a regulated room in the Biomedical Services facility in Oxford University, where the toads were housed. We chose *Xenopus* oocytes to study the macroscopic currents responses elicited by ACh, cytisine or 10-methylcytisine in the $\alpha7$ or $\alpha4\beta2$ nAChR because this system has been widely used for studying ion channels in a controlled *in vivo* environment since it's development by Miledi and colleagues (Barnard et al., 1982). Adult female *Xenopus laevis* were purchased from *Xenopus* 1 (MI, USA) or Nasco (WI, USA). *Xenopus* toads were housed in a climate-controlled, light-regulated room. 50 toads were used. Toads were anaesthetized by immersion in 0.5% tricaine until no-responsive to toe pinch. Toads were then decapitated, and ovarian lobes were harvested and then incubated in 2 mg/ml collagenase Type IA at room temperature for 2 h to isolate and defolliculate oocytes. The collagenase incubation procedure was carried out in a solution (OR2) containing 82 mM NaCl, 2 mM KCl, 2 mM MgCl$_2$, 5 mM HEPES; pH 7.6. Oocytes were maintained until use at 18°C in the same solution (minus collagenase), supplemented with 20mg/ml of neomycin, 100 IU/ml penicillin and 100mg/ml streptomycin.

2.3 Single point mutations

Mutations were introduced in the $\alpha7$, $\alpha4$ or $\beta2$ nAChR subunits using the Stratagene QuikChange Site-Directed Mutagenesis Kit (Agilent, UK). The presence of the mutation and the absence of unwanted mutations were confirmed by sequencing the entire cDNA insert (Eurofins, UK). Note that we present the numbering of the residues according to the full length of the following UniProt sequence codes for human $\alpha4$, $\beta2$ and $\alpha7$ subunits, respectively: P43681 (α4 subunit), P17787 (β2 subunit) and P36544 (α7 subunit). To obtain the position in the mature form, subtract 28 from the number for α4, 25 for β2 and 22 from the $\alpha7$ subunit.

2.4 *Xenopus* oocytes: expression of nAChR and two-electrode voltage clamp recordings

Electrophysiological experiments were carried out with wild type or mutant human $\alpha7$ and $\alpha4\beta2$ nAChR expressed heterologously in *Xenopus* oocytes. Oocytes were injected with $\alpha7$ or $\alpha4$ and $\beta2$ cDNAs, and

recorded using standard procedures, as described previously (Moroni et al., 2008; Rego-Campello et al., 2018). We expressed the two stoichiometries of the $\alpha4\beta2$ nAChR. For the stoichiometry $(\alpha4)_3(\beta2)_2$, a mixture of 10 α4:1 β2 cDNAs was injected into the nucleus of oocytes, whereas for the $(\alpha4)_2(\beta2)_3$ subtype the cDNA ratio injected was 1 α4:10 β2. α7 cDNA was co-injected with chaperone NACHO at a ratio of 1 $\alpha7$: 0.01 NACHO. Receptor expression was examined at least two days later, as previously described (Rego-Campello et al., 2018).

Oocytes were impaled with two electrodes filled with 3 M KCl, and their membrane potential was maintained at -60 mV throughout the experiment. All recordings were performed at 18°C, and cells were perfused with OR2 solution at pH 7.4. Currents were recorded using an automated platform equipped with standard two electrode voltage-clamp configuration (HiClamp; Multi Channel Systems, Reutlignen, Germany). This system differs from standard electrophysiology and other automated platforms because, instead of applying the compound in the perfusion, the oocyte is moved into a well from a 96-well microtiter plate containing 230 μl of the desired solution. Experiments were carried out only if the resting potential of the impaled oocytes was greater than -10 mV and the total holding current less than 0.2 μA. Data were filtered at 10 Hz, captured at 100 Hz using proprietary data acquisition and analysis software running under Matlab (Mathworks Inc., Natick, MA). ACh, cytisine or 10-methylcytisine were prepared as concentrated stock solutions in water and then diluted in the recording medium to obtain the desired test concentrations. Agonist responses were determined using a protocol of 8-12 concentrations with a reference response (1 mM ACh, a fully efficacious ACh concentration at the three wild type nAChR tested) before and after compound testing. A complete experiment on a single oocyte comprised all initial control applications as well as the full planned concentration-response relationship for the agonist tested. To ensure reproducibility of agonist-evoked current amplitudes, three or four initial control applications of 1 mM ACh were carried out. Following the initial control applications, the actual concentration-response relationships of the agonists were obtained. The agonists were applied for 5 s and the washing period between applications was 5 min.

Concentration-activation curve data were fitted with the Hill equation: $y = I_{max}/[1/(EC_{50}/[agonist])^{nH}]$, where y is the normalised current amplitude, Imax is the maximal response (I_{max}/I_{AChMax}), EC_{50} is the agonist concentration at half-maximal efficacy, [agonist] is the agonist concentration, and nH is the Hill coefficient. Curve fitting was carried out using the least-squares method in MATLAB or using GraphPad software version 5. For compounds that elicited less than 100 nA in response to 1-5 mM ACh, the EC_{50} was not determined, and the relative efficacy was established by using the equation: maximal response to test compound/maximal ACh response. Given the very low efficacy of cytisine and 10-methylcytisine at the $\alpha4\beta2$ nAChR (Rego-Campello et al., 2018) and its high affinity for this receptor type, this compound competitively inhibits the ACh responses of $\alpha4\beta2$ nAChR; this property can be used to obtain a measure of the ability of this compound to bind the receptors. Therefore, we determined the concentration-

response curve for the inhibition of current responses elicited by EC_{80} ACh concentrations [30 µM for $(\alpha 4)_2(\beta 2)_3$ or 300 µM for $(\alpha 4)_3(\beta 2)_2$] (see Table S2). The peak of the current responses was normalised to the appropriate EC_{80} ACh concentration. The data were fitted with the Hill equation as described above. Data points for all concentration-response plots represent the mean ± standard error of the mean (SEM) of 8-12 experiments carried out in at least five different batches of oocytes donors. The estimated EC_{50} or IC_{50} values are shown as mean ± 95% CI. The values for I_{max}/I_{AChMax} are shown as mean ± SEM.

The desensitisation rate was estimated from the decay rate of the macroscopic currents. Macroscopic current decays were fitted over the period from the point just after the peak inward current to the end of the drug application period. For $\alpha 7$ and $\alpha 7G174D$ receptors, the agonist (ACh) was applied for 5 s but for receptors with slower decay ($\alpha 7R101A$), the agonist was applied for 7-8 s. Generally, currents were elicited by a saturating concentration of ACh (1 mM ACh for $\alpha 7$ or $\alpha 7G174D$; 3 mM ACh for $\alpha 7R101A$). The decay from the peak to steady-state inward current response was fitted with a bi-exponential expression using GraphPad, software version 5: $f(t)=Af^{-t/\tau f} + As^{-t/\tau s} + C$, where f(t) is the macroscopic current amplitude at any given time, Af is the magnitude of the fast decay component, corresponding to fast desensitisation, and characterized by time constant τf, As is the magnitude of the slower component corresponding to the slow desensitization process characterized by time constant τs, and C is the steady-state current.

2.5 Single-channel recordings from mammalian cells

Single-channel currents were recorded from BOSC 23 cells co-transfected with α7 subunit (wild type or mutant) cDNA and the chaperone Ric-3 cDNA (1:4) by calcium phosphate precipitation. GFP cDNA (5 % of total cDNA amount) was incorporated during the transfection to allow identification of transfected cells. All transfections were carried out for about 8-12 hours in DMEM medium supplemented with 10% FBS, as previously described (Bouzat et al., 2008; Nielsen et al., 2018). Recordings were obtained in the cell-attached patch-clamp configuration at -70 mV. The bath and pipette solutions contained 142 mM KCl, 5.4 mM NaCl, 1.8 mM $CaCl_2$, 1.7 mM $MgCl_2$ and 10 mM HEPES (pH 7.4). We evaluated the effect of ACh and cytisine on the wild type or mutant α7 receptors at approximately their EC_{50} concentrations, which were determined from macroscopic concentration-response curves obtained from the two-electrode voltage-clamp recordings carried out on oocytes described above. The agonist concentrations were as follows. For $\alpha 7$: 100 µM ACh, 25 µM cytisine; for $\alpha 7G174D$: 100 µM ACh, 10 µM cytisine; for $\alpha 7R101A$: ACh, 500 µM, cytisine 500 µM. The agonists were present in the pipette solution, and typical recordings lasted 5-10 minutes. We did not test 10-methylcytisine due to its very low activity at the α7 nAChR (see Table 1). Single-channel currents were digitised at 5-10 µs intervals, low-pass filtered at a cut-off frequency of 10 kHz using an Axopatch 200B patch-clamp amplifier (Molecular Devices, CA, USA) and analysed using the program TAC (Bruxton Corporation, Seattle, WA, USA) with the Gaussian digital filter at 9 kHz (final cut-off frequency 6.7 kHz). Events were detected by the half-amplitude threshold criterion

(Bouzat et al., 2008). To determine channel amplitude, events were tracked regardless of current amplitude, and amplitude histograms were then constructed only for events longer than 0.3 ms to allow full resolution of α7 amplitude (Bouzat et al., 2008; Nielsen et al., 2018). Open-time histograms were fitted by the sum of exponential functions by maximum likelihood using the program TACFit (Bruxton Corporation, Seattle, WA, USA). Bursts of channel openings were identified as a series of closely separated openings preceded and followed by closings longer than a critical duration, the point of intersection between closed components corresponding to intra- and inter-bursts closings (Bouzat et al., 2008; Nielsen et al., 2018). Thus, critical durations were defined by the intersection between the first and second briefest components in the closed-time histogram for bursts of α7 or α7G174D (~200-400 μs), and the intersection between the second and third closed components for bursts of α7R101A (~2-5 ms). These durations were selected in order to avoid artefactual prolongation of burst duration in recordings with high levels of activity. As shown in Figure S2, changes in burst durations were not found for α7G174D if the critical time was defined by the intersection between the first and second closed components (ACh: 0.69 ± 0.17 ms; Cyt: 1.25 ± 0.30 ms), or the second and third closed components (ACh: 0.72 ± 0.16 ms; Cyt: 1.22 ± 0.06 ms: $p > 0.05$ in both cases). The longest duration closed components were not considered for the analysis since they vary with the level of expression of α7 nAChR in each cell. Each patch corresponds to a different cell (n indicates the number of independent experiments). For each condition (distinct receptors or agonists), recordings were performed from three or more different cell transfections in different days (N indicates the number of cell transfections). Estimated parameters represent the mean ± standard deviation (SD).

2.6 Radioligand binding studies

[³H]Epibatidine binding assays were carried out on membrane homogenates prepared from HEK 293 cells transfected with α4 and β2 cDNAs, as previously reported (Rego-Campello et al., 2018). For saturation experiments, the membrane homogenate aliquots were incubated overnight at 4 °C with 0.01-2.5 nM concentrations of (±)-[³H]epibatidine. Nonspecific binding was determined in parallel by adding to the incubation solutions 100 nM unlabelled epibatidine. At the end of the incubation, the samples were filtered on a GFC filter soaked in 0.5% polyethylenimine and washed with 15 mL ice-cold phosphate buffered saline (PBS) containing 137 mM NaCl, 2.7 mM KCl, 10 mM Na_2HPO_4, 1.8 mM KH_2PO_4 at pH 7.4. The filters were counted in a β counter. For [¹²⁵I]Bungarotoxin ([¹²⁵I]Bgtx) saturation binding studies were carried out on membrane homogenate prepared from SH-SY5Y cells transfected with human α7 cDNA, as described previously (Rego-Campello et al., 2018). The transfected cells were first washed by centrifugation with PBS supplemented with 2 mM phenylmethylsulfonyl fluoride) and then homogenised in the same buffer. Both saturation and competition binding experiments for [³H]epibatidine or [¹²⁵I]αBgtx were performed using the PBS buffer described above. Aliquots of the membrane homogenates were incubated overnight with 0.1-10.0 nM concentrations of [¹²⁵I]Bgtx at room temperature. Nonspecific binding was determined in parallel by including in the assay mixture 1 μM unlabeled Bgtx. After

incubation, the samples were filtered as described for [³H]epibatidine binding. For competition studies, the inhibition of [³H]epibatidine or [¹²⁵I]Bgtx binding was measured by incubating the membranes transfected with the appropriate subtype with increasing concentrations of cytisine or 10-methylcytisine for five minutes followed by overnight incubation at 4 °C, with 0.1 nM [³H]epibatidine or at room temperature with 2-3 nM [¹²⁵I]Bgtx in the case of the $\alpha 7$ subtype. At the end of the incubation time, the samples were processed as described for the saturation studies. [¹²⁵I]Bgtx binding by measured by direct counting in an α counter.

Saturation binding data were evaluated by one-site competitive binding curve-fitting procedures using GraphPad Prism version 5 (GraphPad Software, CA, USA). In the saturation binding assay, the maximum specific binding (Bmax) and the equilibrium binding constant (Kd) values were calculated using one site–specific binding with Hill slope – model. K_i values were obtained by fitting the competition binding data. Inhibition constants (Ki) were estimated by reference to the Kd of the radioligand, according to the Cheng-Prusoff equation. All assays were carried out in triplicates, and the data shown represent the mean ± SEM of three independent experiments (three different transfected cell batches), each performed in duplicate for each compound on each subtype

2.7 Experimental design and statistical analysis of functional data

The data and statistical analysis comply with the recommendations on experimental design and analysis in pharmacology (Curtis et al., 2018). For *Xenopus* oocyte experiments, the final data sets were assembled from a minimum of 5 independent recordings (i.e., n = 5) conducted on oocytes obtained from at least 5 different *Xenopus* donors (i.e., N = 5). Data obtained from the same batch of oocytes were considered replicates. The data sets represent full concentration-response relationships obtained from individual oocytes (i.e., incomplete experiments were discarded). The data from each experiment were fitted separately, and the estimated EC_{50} values were used to obtain the mean EC_{50} or IC_{50} (95% CI) reported in the manuscript or Supplementary Information. $LogEC_{50}$ values for agonist or inhibition concentration responses, changes in onset of current decay were analysed using one-way ANOVA, followed by a post hoc Dunnett's test and/or a post hoc Bonferroni multiple comparison test to determine the level of significance between wild type and mutant receptors. Prior to the ANOVA analysis, the data were tested for normality using the D'Agostino and Pearson normality test in PRISM and were normally distributed. Post hoc tests were run only if F achieved $P < 0.05$ and there was no significant variance in homogeneity. For data collected from *Xenopus* oocytes, fitting and statistical analyses were blinded. Datasets were coded by the experimenter and then analysed by a member of the team not involved in the injection of oocytes with nAChR subunit DNA or in the two-electrode voltage-clamp recordings. For single-channel recordings or data analysis, blinding was not practical. Single-channel analysis, data sets that passed the Shapiro-Wilk test for normality and the Levene Median test for equal variance were analysed to determine levels of statistical difference using two-tailed Student's *t*-tests for pairwise

comparisons or one-way ANOVA followed by Bonferroni's posthoc tests for multiple comparisons with SigmaPlot 12.0 (Systat Software, Inc.). For all the functional data shown here, differences between wild type and tests were considered statistically different if $p < 0.05$.

2.8 Molecular Dynamics Simulations

Molecular dynamics (MD) simulations of the extracellular domain (ECD) of wild type and mutant human α4β2 or α7 nAChR subtypes were performed to identify the molecular factors that control the selectivity of the C(10) variants of cytisine. The ECD of the human α4β2 nAChR (PDB code: 5KXI) (Morales-Perez et al., 2016) was used as the starting point for all α4β2 systems whereas the homology model of the human α7 nAChR taken from our previous work (Rego-Campello et al., 2018) was the starting point for all α7 simulations. All systems were simulated with ACh, cytisine or 10-methylcytisine bound to two nonconsecutive binding pockets. It has been shown experimentally that the binding of agonists to two nonconsecutive binding pockets enables proper activation of homomeric Cys loop receptors (Bouzat et al., 2009). ACh was placed in the binding pockets in a position analogous to the one observed in the crystal structure of the AChBP from *Aplysia Californica* (PDB code: 2XZ5) (Brams et al., 2011). The binding modes of cytisine and 10-methylcytisine were the same as those previously described (Rego-Campello et al., 2018). The protonation state of the protonatable groups was determined using a combination of Poisson-Boltzmann, and Metropolis Monte Carlo calculations, as previously described (Oliveira et al., 2019). Based on these calculations, all protonatable residues were found to be in their standard state at a physiological pH and the three agonists (ACh, cytisine and 10-methylcytisine) were considered to be positively charged. All MD simulations were performed using Gromacs (version 5.1.4) on the University of Bristol's High-Performance Computer, BlueCrystal (Phase 4) (Abraham et al., 2015). The Amber ff99SB-ILDN (Lindorff- Larsen et al., 2010) force-field was used to describe the protein. The parameters for cytisine and 10-methylcytisine were taken from our previously published work (Rego-Campello et al., 2018). Acpype (Sousa da Silva and Vranken, 2012) was used to generate Amber-GAFF parameters for ACh. All systems were solvated using TIP3P waters (Jorgensen et al., 1983). The simulations were performed at the constant temperature of 310 K, and the velocity-rescaling thermostat was used, with separate couplings for the solutes (protein and agonists) and solvent, using a relaxation time constant of 0.1 ps. A Berendsen barostat was used to keep the pressure at 1 bar, with a coupling constant of 1 ps. A time step of 2 fs was used for integrating the equations of motion. Non-bonded long-range electrostatic interactions were calculated using the smooth particle mesh Ewald method beyond a 12 Å cutoff. The same 12 Å cutoff was used for the van der Waals interactions with long-range dispersion corrections for the energy and pressure. The neighbour lists were updated every 20 steps. All systems were energy minimised, equilibrated and simulated according to the protocol as previously described (Rego-Campello et al., 2018). Five unrestrained MD simulations were performed for each of the following protein-agonist complexes: α4β2, α4β2R106A, α7, α7R101A and α7G174D, each bound to ACh, cytisine or 10-methylcytisine. All systems were energy minimised, equilibrated and simulated according to the

protocol described in (Rego-Campello et al., 2018). Five unrestrained simulations, each 100 ns long, were performed for each protein-agonist complex, in a total of 7.5 µs of simulation. Note that MD inputs and outputs (including the original trajectories) are available upon request.

2.9 Analysis of the MD simulations

All the analyses were performed using Gromacs (Abraham et al., 2015) and in-house tools. Principal component analysis (PCA) was used to examine the sampling of the replicates, as previously described (Oliveira et al., 2019), and identify the differences between wild type and mutant receptors (data available upon request). Each PCA trajectory contained one conformation per nanosecond per replicate (totaling 5001 frames). The two principal components (PC1 and PC2) were used to assess the equilibration/relaxation of the simulations, and all systems were considered equilibrated after 50 ns. The different replicates sampled different regions of conformational, thus improving the overall sampling for each system.

The structural stability of the agonist-bound and unbound receptor complexes was examined by monitoring two system properties- namely, the C_α root mean square deviation (RMSD) from the starting structure and the secondary structure content, as previously described (Oliveira et al., 2019). Both systems remained stable over the simulation time, and the average C_α RMSD profiles showed a plateau after 20 ns (Figures S3; S4). The stability of the systems was further demonstrated by the analysis of the secondary structure content of the receptor using the hydrogen bond estimation algorithm DSSP (Kabsch and Sander, 1983) with only a small secondary structure loss (data not shown).

2.10 Nomenclature of targets and ligands

Key protein targets and ligands in this article are hyperlinked to corresponding entries in **http://www.guidetopharmacology.org**, the common portal for data from the IUPHAR/BPS Guide to PHARMACOLOGY (Harding et al., 2018), and are permanently archived in the Concise Guide to PHARMACOLOGY 2017/18 (Alexander et al., 2017).

3 RESULTS

3.1 An arginine residue in β3-strand affects agonist selectivity

Recently, we suggested that differences in the second layer of residues in the binding pocket of the α7 and α4β2 nAChR may account for the selectivity of 10-methylcytisine (Rego-Campello et al., 2018). These included residues that affect the hydrophobicity (β2F144 *vs* α7Q139), network of hydrogen bonds (β21332S *vs* α7T128 and α4T183 *vs* α7S172) and volume of the binding pocket (β2V136 *vs* α7L131, β2A65 *vs* α7L60). However, functional assays of relevant α7 mutant variants failed to demonstrate the involvement of these residues on the selectivity of 10-methylcytisine (Table S1). Here, we explored the differences between the subtype binding sites by performing MD simulations of α4β2 and α7 nAChR ECD complexes with ACh, cytisine or 10-methylcytisine. Note that 10-methylcytisine represents a relatively modest modification of cytisine with the addition of a sterically undemanding methyl moiety, lacking any polar component capable of interacting with other residues.

MD simulations revealed distinct patterns of dynamical behaviour of the agonists bound to α7 or α4β2 nAChR. In the α4β2 complexes, ACh exhibited high mobility, adopting many different binding modes in the agonist binding pocket (Figure 1B). As expected from their more rigid structures and additional cation-π interaction with loop C compared to ACh (Blom et al., 2019), cytisine and 10-methylcytisine showed less mobility, generally remaining in the same orientation throughout the simulation. In the α7 complexes, all agonists exhibited greater positional and conformational variability, regardless of the steric bulk and rigidity of the ligands (Figure 1B).

The MD simulations led us to identify an arginine residue located in β3-strand of the α7 (R101) and β2 (R106) subunits as key in distinguishing α7 from α4β2 (Figures 2A, 2B; Figures S5, S6). The β3-strand arginine is conserved in the nAChR family (Figure S7) and has been reported to affect agonist potency in bovine α7 nAChR (Criado et al., 2011).

In the α7 complex, the side chain of R101 was highly mobile (Figure 2A; Figure S5; Movie 1) as it lacked a nearby negatively charged residue to form stable electrostatic interactions with (Figure 2A). While sampling the space, the side chain of R101 oriented downward towards the inside of the binding pocket establishing transient interactions with loop C residues, notably with E215 (Figure 3A). The side chain of R101 was even able to approach the C(10) position of the cytisine scaffold, which in the 10-methylcytisine-α7 complex resulted in the loss of interactions between 10-methylcytisine and loop C residues Y210 (TyrC1) and Y217 (TyrC2) of the agonist binding pocket (Figures 2C, 2D; Movie 1). (See Figure S1A for a model of the agonist binding pocket in nAChR).

In contrast, in $\alpha 4\beta 2$ nAChR, $\beta 2$R106 was less mobile as it established a salt-bridge with an aspartate residue ($\alpha 4$D185) from loop B (Figures 2B, 3B; Figures S5) and only transiently with a glutamate residue in loop C ($\alpha 4$E228) that is equivalent to $\alpha 7$E215 (Figure 3C). The aspartate residue in loop B is not conserved in the $\alpha 7$ subtype (Figure S7). While the salt-bridge between $\alpha 4$D185 and $\beta 2$R106 was stable during the simulation (Figure 3B), the interaction with $\alpha 4$E228 was less frequent than that of its counterpart in the $\alpha 7$ complex (R101-E215) (Figures 3A, 3C). Two-electrode voltage recordings from *Xenopus* oocytes expressing $\alpha 4$D185G$\beta 2$ or $\alpha 4\beta 2$R106A receptors revealed reduced functional expression without changes in agonist potency (n = 10; N = 5; p < 0.05) (Table S2). In line with these findings, [^{3}H]epibatidine binding assays showed that D185G reduced maximal binding (Bmax) without changes in binding affinity (K_d) (N = 3) (Table S2).

3.2 The conserved $\beta 3$-strand arginine influences agonist binding and function in $\alpha 7$ nAChR

Given that TyrC1 and TyrC2 are essential for ligand binding affinity in $\alpha 7$ (Corringer et al., 1995; Puskar et al., 2011; Huang et al., 2013), we speculated that the loss of the interactions with these tyrosine residues could explain the negligible affinity of 10-methylcytisine for the $\alpha 7$ subtype. Our aim was to mimic the $\alpha 4\beta 2$ salt-bridge between $\beta 2$R106 and $\alpha 4$D185 in $\alpha 7$, by mutating $\alpha 7$G174 to aspartate ($\alpha 7$G174D) to allow a salt-bridge to form with R101. MD simulations of $\alpha 7$G174D showed that R101 forms an inter-subunit salt-bridge with G174D (Figure 4A). This salt-bridge not only influenced the correlated motions (Figure S8) and fluctuations (Figure S9) of the subunits but also reduced the frequency of the interaction between R101 and E215 of loop C (Figure 4B). G174D also induced ligand-dependent changes in the distribution of the distances between the ligands and the conserved aromatic residues of the agonist binding pocket, particularly with $\alpha 7$Y115 (TyrA) and $\alpha 7$W77 (TrpD) (Figure 4C, 4D; Figure S10). This finding is significant because TyrA and TrpD are pivotal for the binding mode of agonists in the $\alpha 7$ subtype (Horenstein et al., 2008; Williams et al., 2009; Puskar et al., 2011; Arnam et al., 2013).

To assess the functional impact of G174D on agonist effects, we obtained activation concentration-response curves for ACh and the cytisine compounds from $\alpha 7$G174D receptors expressed in *Xenopus* oocytes. As shown in Figure 5A and Table 1, G174D increased the potency of cytisine and 10-methylcytisine but had no effects on ACh function (Table 1). The amplitude of the maximal responses of cytisine was similar to that of the maximal responses of $\alpha 7$ receptors but that of 10-methylcytisine almost doubled (Table 1). Saturation [^{125}I]αBgtx binding assays suggested G174D had no effects on the binding affinity ($\alpha 7$ K_d 0.32 ± 0.13 nM; $\alpha 7$G174D K_d 0.33 ± 0.10 nM; n = 3; N =3) or the maximal binding capacity (B_{max}) ($\alpha 7$, 463 ± 133 fmol/mg prot; $\alpha 7$G174D, 430 ± 165 fmol/mg prot; n = 3; N =3). However, competition assays suggested that G174D enhances the ability of cytisine and 10-methylcytisine to displace [^{125}I]αBgtx binding (cytisine K_i: $\alpha 7$, 855 ±350 nM; $\alpha 7$G174D, 169 ± 66 nM (n = 3; N = 3). 10-

methylcytisine K_i: $\alpha7$, 5371 ± 2200 nM; $\alpha7$G174D, 458 ±320 (n = 3; N = 3). Therefore, the G174D-R101 salt-bridge enhances the binding affinity and functional potency of cytisine and 10-methylcytisine but has not effect on [^{125}I]αBgtx maximal binding.

We further examined the role of R101 in agonist binding by reversing the charge at R101 (via R101D) and swapping the charge at G174D (via G174R) to potentially restore the salt-bridge. R101D drastically reduced the amplitude of currents elicited by saturating ACh concentrations: the amplitude of the current responses to 1, 3 or 5mM ACh was comparable and on average, no greater than 70 nA (Table 1). G174R,R101D did not reverse the effects of R101D (Table 1), indicating that charge reversal is not well tolerated at position R101. R101K and G174E also decreased agonist potency but double mutant G174E,R101K restored agonist potency, compared to G174D (Figure 5B, Table 1). Given that the stability of salt-bridges is affected by the distance between the bridging residues, the changes in agonist potency at $\alpha7$G174E,R101K, $\alpha7$G174E and $\alpha7$G174D,R101K may reflect the variation in the length of the side chain of the residues involved (Figure 5C).

3.3 G174D increases the duration of activation episodes in $\alpha7$ nAChR

To decipher the effect of G174D on agonist action at the molecular level, we performed cell-attached patches in the presence of EC_{50} ACh or cytisine (For $\alpha7$: 100 μM ACh, 25 μM cytisine; for $\alpha7$G174D: 100 μM ACh, 10 μM cytisine) in the pipette solution. We did not test 10-methylcytisine due to its very low activity and potency at the $\alpha7$ nAChR (Table 1) (Rego-Campello et al., 2018). For α7 nAChR, ACh or cytisine single-channel activity appeared as single brief pulses flanked by long-closed periods or occasionally as bursts of several openings in quick succession (Figure 6A), which correspond to activation episodes of a single receptor molecule (Bouzat et al., 2008; Nielsen et al., 2018). A wide range of channel amplitudes are detected because the brief open-channel lifetime does not allow full amplitude resolution (Bouzat et al., 2008). Amplitude histograms for events longer than 0.3 ms that were fully resolved yielded a mean value of ~10 pA (9.99 ± 0.41 pA) for both agonists, in agreement with previously published data for ACh (Bouzat et al., 2008; Nielsen et al., 2018). Whilst there were no statistically significant differences in the mean open duration of α7 receptors activated by ACh or cytisine 1 (~0.28 ms), the burst duration in the presence of cytisine was significantly longer (~0.72 ms) than in the presence of ACh (~0.33 ms) (Figure 6B; Table S3). This finding is in line with the greater sensitivity of $\alpha7$ receptors to activation by cytisine, compared to ACh. For α7G174D nAChR, the single-channel amplitude (10.01 ± 0.26 pA) and the mean open duration for ACh or cytisine were comparable to wild type (Figure 6B, Table S3). However, for both agonists, the mean burst durations increased by ~2 fold, compared to wild type (Figure 6B, Table S3). A likely explanation for the increased burst duration could be that G174D slows desensitisation. Desensitisation has been suggested as the predominant pathway for channel closing and burst termination in $\alpha7$ receptors (Bouzat et al., 2008). Although the rate of desensitisation of $\alpha7$ receptors cannot be accurately determined from the decay rate of macroscopic currents, particularly when

using relatively slow temporal systems (Bouzat et al., 2008), a change in the desensitisation rate should translate to a change in the decay rate. The continuous application of a saturating concentration of ACh (1mM) to oocytes expressing either wild type or α7G174D receptors induced current responses that decayed rapidly from their peaks (Figure 6C). The onset for desensitisation for α7 receptors expressed in *Xenopus* oocytes (Khiroug et al., 2002; Gay et al., 2008) or CHO cells (McCormack et al., 2010) has been shown to be biphasic; we found that the fast (τf) and slow (τs) time constants of the decays were similar for both receptors (α7: τf, 223 ± 77 ms, τs 1.4 ± 0.4 s; α7G174D: τf 270 ± 50 ms, τs 0.9 ±0.2 s; n =10, N = 6) and comparable to previously published constants under similar conditions (Khiroug et al., 2002; McCormack et al., 2010). Thus, desensitisation is not mediating the increased burst duration in the mutant receptor. An alternative explanation consistent with the findings from the MD simulations and the functional results might be that a decrease in R101 mobility through a *de novo* salt bridge in the α7G174D mutant allows agonists, particularly bulky agonists such as cytisine and 10-methylcytisine, to adopt positions within the binding site that favour interactions with core-binding residues (e.g., TyrA, TyrC and TrpD). These interactions may increase the stabilization of the agonist and/or enhance the efficacy for activation, allowing α7G174D to activate in episodes or bursts that otherwise are very infrequent in α7 receptors.

3.4 α7R101A affects agonist potency, burst duration and onset of current decay

We further examined the effect of R101 on receptor function by neutralizing the charge of this residue (i.e., R101A). As shown in Figure 7A and Table 1, R101A decreased the potency of all agonists tested. The greatest decrease was observed for ACh and cytisine (~11 fold). Furthermore, R101A caused a ~4-fold increase in the relative efficacy of cytisine (Table 1).   R101A increased the fast and slow time constants for the onset of desensitisation: τf = α7, 223 ± 77 ms vs α7R101A, 1.01 ± 0.05 s, n = 10; N = 6, p < 0.05); τs = α7, 1.4 ± 0.4 s vs α7R101A, 2.7 ± 0.8 s; n = 10, N = 5, p < 0.05) (Figure 7B).

R101A had no effects on the amplitudes of the single-channel currents elicited by EC_{50} ACh (α7: 100 μM; α7R101A: 500 μM) or cytisine (α7: 25 μM; α7R101A: 500 μM), compared to wild type (10.12 ± 0.26 pA and 9.99 ± 0.41 pA, respectively, n = 8; N = 5). Also, R101A had no effects on the mean open duration of the single currents activated by either agonist (Figure 7B; Table S3). However, R101A increased the mean burst duration by ~3-to 4-fold, compared to wild type and, surprisingly, by 2-fold compared to G174D (Figure 7C; Table S3). The increase in burst duration may be a consequence of the slower desensitisation of α7R101A, as bursts in α7 nAChR terminate by desensitisation (Bouzat et al., 2008). However, given that R101 also affected potency, we cannot discard the possibility that changes in agonist binding and/or gating contributed to the increased burst duration and changes in desensitisation. Indeed, the majority of the mutations of pLGIC previously reported as affecting desensitisation, also strongly alter the activation and gating of the receptor, with controversial and ambiguous results (Gielen and Corringer, 2018).

For all three agonists, analysis of the Root Mean Square Fluctuations (RMSF) profiles of the Cα atoms between α7 and α7R101A showed differences in the binding site region and structural motifs involved in inter-domain communication. In the ACh-bound complexes, the largest differences are located in loops A, B and Cys loop (Figure 8; Figure S11). In complexes involving cytisine, the most noticeable differences are observed in loops A, B, E and F and loop Cys (Figure 8; Figure S11). In 10-methylcytisine complexes, the differences are in loops C, D, E and F and loop Cys (Figure 8; Figure S11).

The comparison between the average structures of α7 and α7R101A highlighted structural differences in loops C and F mainly when in the presence of the bulkier ligands (Figure 9; Figure S12). The difference in the loop C region is likely due to the loss of the electrostatic interaction between R101 and E215 in loop C. This interaction affects agonist function, as suggested by the reduced potency of all three ligands at α7E215A receptors (Table 1). To compensate for the loss of the E215-R101 interaction in α7R101, E215 (very) transiently formed a salt-bridge with K98 (located close to R101) (Figure S13). Analysis of the distribution of the distance between agonists and the conserved aromatic residues of the agonist pocket were similar for all three agonists, except for TyrA, which for cytisine varied between the α7 and α7R101A systems (Figure S14). For cytisine, the agonist most affected by mutations E215A or R101A (see Table 1), the (low) frequency of this new interaction affects the closing of loop C (Figure 9; Figure S12).

4 DISCUSSION

For the purpose of developing partial agonists for the $\alpha4\beta2$ nAChR with improved selectivity, we generated a range of diverse and enantiomerically pure C(10) variants of cytisine, exemplified (-)-10-methylcytisine (Rego-Campello et al., 2018). These variants consistently display increased affinity for $\alpha4\beta2$ but, despite the more permissive nature of the agonist binding pocket of the $\alpha7$ nAChR (Horenstein et al., 2008), they exhibit negligible affinity for this subtype (Rego-Campello et al., 2018). Here, we identify a conserved arginine in $\beta3$-strand as key in determining the negligible affinity of 10-methylcytisine for $\alpha7$ nAChR. In the $\alpha4\beta2$ subtype, the homologous $\beta2R106$ is stabilized through an inter-subunit salt-bridge, which is necessary for receptor expression but has no effect on agonist effects. In contrast, in the $\alpha7$ nAChR, the arginine residue, which is not stabilised by electrostatic interactions, is highly mobile. For cytisine and 10-methylcytisine, this mobility leads to steric clashes that manifest as competition for the space associated with the agonist binding site. For 10-methylcytisine, this weakens the interaction with TyrC1 and TyrC2 in loop C, which ultimately ablates the binding of this ligand. When the mobility of R101 is reduced through a salt-bridge with G174D, all agonists achieve optimal binding interactions with core agonist binding residues (i.e., TyrA, TyrC1, TyrC2 and TrpD), depending on the steric bulk and the binding mode of the agonist. These interactions likely increase the strength of agonist binding and/or enhance the efficacy for activation, allowing $\alpha7G174D$ to activate in episodes or bursts that are very infrequent in $\alpha7$ nAChR. Our MD simulations, together with the potency of agonists in the $\alpha7E215A$ receptors, suggest that the interaction of R101 with E215 in loop C may shape the dynamical behavior of loop C, which in $\alpha7R101A$, and for bulkier ligands like cytisine, can impact loop C capping. The role of loop C capping in channel gating is still under debate (Purohit and Auerbach, 2013) but its role in anchoring bound agonist to the binding site is well established (Auerbach, 2015). Thus, the R101-E215 interaction may be a pivotal component of the R101-loop C mechanism influencing agonist binding affinity in the $\alpha7$ nAChR.

In addition to agonist binding residues, R101 also influences the dynamical behaviour of the Cys loop. The Cys loop has been suggested to be involved in propagating coupling signals in the $\alpha7$ nAChR (Oliveira et al., 2019) and residues in this region have been implicated in achieving maximal response to agonists (Grutter et al., 2005; Jha et al., 2007; Lee et al., 2009; Yan et al., 2015). In accord with these studies, we found that R101A increased the relative efficacy of cytisine, a change that could be due to modifications in gating driven by changes in the dynamical behaviour of the Cys loop. Changes in gating could also underlie burst prolongation in $\alpha7R101A$. We have shown previously that bursts in the $\alpha7$ receptor are terminated by desensitisation (Bouzat et al., 2008). The slower decay rate observed for $\alpha7R101A$ may be correlated with a macroscopic slower desensitisation rate, despite the slow temporal resolution of the *Xenopus* oocyte system. The structural elements underpinning desensitisation in the $\alpha7$ nAChR have not been fully identified but the majority of the mutations of Cys loop neurotransmitter-gated

ion channels previously reported as affecting desensitisation, also strongly alter the activation and gating of the receptor (Revah et al., 1991; Auerbach and Akk, 1998; Zhang et al., 2011; Gielen and Corringer, 2018). However, changes in efficacy and desensitisation may stem from the influence of R101 on agonist binding. Unsurprisingly, mutations in TrpD (Gay et al., 2008) and a residue between two binding loops (McCormack et al., 2010) have been found to influence desensitisation of the α7 nAChR. Whether R101 modulates the behavior of theCys loop and/or agonist binding residues, thus influencing efficacy, burst duration, and desensitisation represents an important question for future studies.

Besides the very transient E215-R101 interaction, our studies did not reveal any specific pairwise electrostatic interactions for R101. Due to the motility of its side chain, R101 dominates the electrostatic landscape surrounding the binding pocket (Figure S15) and, as suggested by the functional consequences of charge reversal or charge neutralization of R101, the overall charge of this region is critical for the function of the α7 nAChR. R101 may exert its multifarious effects on α7 receptors by providing the electrostatic background on which critical agonist-binding and gating interactions occur. In α4β2, R106 also contributes to the overall charge around the agonist site but has no impact on function. This may be due to the reduced dynamics of the side chain of R101 as it is involved in a strong inter-subunit salt-bridge with D185. In the α7 nAChR, the high motility of the side chain of R101 allows it to even orient towards the inside of the binding pocket, which may further impact the electrostatic enviroment inthese region. Our observations add further support to the body of evidence that indicates the crucial role of overall charge for Cys loop receptor function (Carpenter and Lightstone, 2016), (Meltzer et al., 2006), (Azam et al., 2015) and (Xiu et al., 2005).

In the α4β2 nAChR, R106 is stabilized through an inter-subunit salt bridge with an aspartate residue in loop B of the α4 subunit (α4D185). The salt-bridge has no impact on agonist selectivity but is necessary for functional expression. This finding suggests a role in receptor biogenesis, as is the case for an equivalent arginine residue in the GABA$_A$ receptor (Hales et al., 2005). The salt-bridge between the arginine in β3-strand and the aspartate in loop B is highly conserved among heteromeric nAChRs (Figure S7). In the nAChR family, which shows a high degree of sequence conservation in the agonist binding site, functional divergence was largely achieved through heteromeric receptors (Marcovich et al., 2020). In this context, and considering that salt-bridges bring stability to multimeric protein ensembles (Sokalingam et al., 2012), one can speculate that the salt-bridge between the β3-strand arginine and loop B aspartate emerged during the evolution of nAChR to aid the stabilisation of heteromeric receptor ensembles.

Conclusion and clinical significance

We show that an R101 in β3-strand of the α7 nAChR modulates the binding of cytisine and 10-methylcytisine. Why is this significant? The primary target for current smoking cessation drugs such as cytisine and varenicline is the α4β2 nAChR. Despite the proven efficacy of these drugs, off-target psychiatric effects are problematic, and relapse rates are high, and this may be partly due to the broad nAChR selectivity of these compounds, which includes the α7 subtype. Suppression of activity in non-targeted nAChR, such as the α7 subtype, thus remains a key step towards more efficacious smoking cessation pharmacotherapies and our findings offer a clear path towards this goal.

CONFLICT OF INTEREST

The authors declare no conflict of interest.

AUTHORS CONTRIBUTION

CB, CG, DKS, RBS, AJM, IB, ASO designed research. TM, BEN, CG, IB, ASO performed research and analysed data. IB, TG, ASO, SW, AJM, CB, BEN wrote paper. IB, CB provided supervision.

DECLARATION OF TRANSPARENCY AND SCIENTIFIC RIGOUR

This Declaration acknowledges that this paper adheres to the principles for transparent reporting and scientific rigour of preclinical research as stated in the *BJP* guidelines for **Design & Analysis** and as recommended by funding agencies, publishers, and other organisations engaged with supporting research.

REFERENCES

Abraham, M.J., Murtola, T., Schulz, R., Páll, S., Smith, J.C., Hess, B., et al. (2015). GROMACS: High performance molecular simulations through multi-level parallelism from laptops to supercomputers. *SoftwareX 1–2*: 19–25.

Alexander, S.P., Kelly, E., Marrion, N.V., Peters, J.A., Faccenda, E., Harding, S.D., et al. (2017). THE CONCISE GUIDE TO PHARMACOLOGY 2017/18: Overview. *British Journal of Pharmacology 174*: S1–S16.

Arnam, E.B.V., Blythe, E.E., Lester, H.A., and Dougherty, D.A. (2013). An Unusual Pattern of Ligand-Receptor Interactions for the α7 Nicotinic Acetylcholine Receptor, with Implications for the Binding of Varenicline. *Molecular Pharmacol*ogy *84*: 201–207.

Auerbach, A. (2015). Agonist activation of a nicotinic acetylcholine receptor. *Neuropharmacology 96*: 150–156.

Auerbach, A., and Akk, G. (1998). Desensitisation of Mouse Nicotinic Acetylcholine Receptor Channels : A Two-Gate Mechanism. Journal of General Physiology *112*: 181–197.

Azam, L., Papakyriakou, A., Zouridakis, M., Giastas, P., Tzartos, S.J., and McIntosh, J.M. (2015). Molecular Interaction of α-Conotoxin RgIA with the Rat α9α10 Nicotinic Acetylcholine Receptor. *Molecular Pharmacology 87*: 855–864.

Barnard, E.A., Miledi, R., and Sumikawa, K. (1982). Translation of exogenous messenger RNA coding for nicotinic acetylcholine receptors produces functional receptors in Xenopus oocytes. *Proceedings of the Royal Society of London. Series B. Biological Sciences 215*: 241–246.

Blom, A.E.M., Campello, H.R., Lester, H.A., Gallagher, T., and Dougherty, D.A. (2019). Probing Binding Interactions of Cytisine Derivatives to the α4β2 Nicotinic Acetylcholine Receptor. *Journal of the American Chemical Society 141*: 15840–15849.

Bouzat, C., Bartos, M., Corradi, J., and Sine, S.M. (2008). The Interface between Extracellular and Transmembrane Domains of Homomeric Cys-Loop Receptors Governs Open-Channel Lifetime and Rate of Desensitisation. Journal of Neuroscience *28*: 7808–7819.

Bouzat, C.B., Rayes, D., Rosa, M.J.D., and Sine, S.M. (2009). Electrical Fingerprinting Reveals Agonist Binding Sites Required for Activation of Homo-pentameric Cys-loop Receptors. *Biophysical Journal 96*: 167a.

Brams, M., Gay, E.A., Sáez, J.C., Guskov, A., Elk, R. van, Schors, R.C. van der, et al. (2011). Crystal Structures of a Cysteine-modified Mutant in Loop D of Acetylcholine-binding Protein. *Journal of Biological Chemistry 286*: 4420–4428.

Carpenter, T.S., and Lightstone, F.C. (2016). An Electrostatic Funnel in the GABA-Binding Pathway. *PLOS Computational Biology 12*: e1004831.

Coe, J.W., Rollema, H., and O'Neill, B.T. (2009). Chapter 4 Case History: Chantix™/Champix™ (Varenicline Tartrate), a Nicotinic Acetylcholine Receptor Partial Agonist as a Smoking Cessation Aid. *In Annual Reports in Medicinal Chemistry*, J.E. Macor, ed. (Academic Press), pp 71–101.

Corringer, P.-J., Galzi, J.-L., Eiselé, J.-L., Bertrand, S., Changeux, J.-P., and Bertrand, D. (1995). Identification of a New Component of the Agonist Binding Site of the Nicotinic 7 Homooligomeric Receptor. *Journal of Biological Chemistry 270*: 11749–11752.

Corringer, P.-J., Novère, N.L., and Changeux, J.-P. (2000). Nicotinic Receptors at the Amino Acid Level. *Annual Review of Pharmacology and Toxicology 40*: 431–458.

Criado, M., Mulet, J., Gerber, S., Sala, S., and Sala, F. (2011). Mutants of β-strand β3 and the loop B in the interface between α7 subunits of a homomeric acetylcholine receptor show functional and pharmacological alterations. *Journal of Neurochemistry 118*: 968–978.

Curtis, M.J., Alexander, S., Cirino, G., Docherty, J.R., George, C.H., Giembycz, M.A., et al. (2018). Experimental design and analysis and their reporting II: updated and simplified guidance for authors and peer reviewers. *British Journal of Pharmacology 175*: 987–993.

Dineley, K.T., Pandya, A.A., and Yakel, J.L. (2015). Nicotinic ACh receptors as therapeutic targets in CNS disorders. T*rends in Pharmacological Sciences 36*: 96–108.

Gay, E.A., Giniatullin, R., Skorinkin, A., and Yakel, J.L. (2008). Aromatic residues at position 55 of rat α7 nicotinic acetylcholine receptors are critical for maintaining rapid desensitisation. *The Journal of Physiology 586*: 1105–1115.

Gielen, M., and Corringer, P.-J. (2018). The dual-gate model for pentameric ligand-gated ion channels activation and desensitisation. *The Journal of Physiology 596*: 1873–1902.

Gotti, C., Clementi, F., Fornari, A., Gaimarri, A., Guiducci, S., Manfredi, I., et al. (2009). Structural and functional diversity of native brain neuronal nicotinic receptors. *Biochemical Pharmacology 78*: 703–711.

Grutter, T., Carvalho, L.P. de, Dufresne, V., Taly, A., Edelstein, S.J., and Changeux, J.-P. (2005). Molecular tuning of fast gating in pentameric ligand-gated ion channels. *Proceedings of the National Academy of Sciences USA 102*: 18207–18212.

Hajek, P., McRobbie, H., and Myers, K. (2013a). Efficacy of cytisine in helping smokers quit: systematic review and meta-analysis. *Thorax 68*: 1037–1042.

Hajek, P., Stead, L.F., West, R., Jarvis, M., Hartmann-Boyce, J., and Lancaster, T. (2013b). Relapse prevention interventions for smoking cessation. *Cochrane Database of Systematic Reviews*.

Hales, T.G., Tang, H., Bollan, K.A., Johnson, S.J., King, D.P., McDonald, N.A., et al. (2005). The epilepsy mutation, γ2(R43Q) disrupts a highly conserved inter-subunit contact site, perturbing the biogenesis of GABAA receptors. *Molecular and Cellular Neuroscience 29*: 120–127.

Harding, S.D., Sharman, J.L., Faccenda, E., Southan, C., Pawson, A.J., Ireland, S., et al. (2018). The IUPHAR/BPS Guide to PHARMACOLOGY in 2018: updates and expansion to encompass the new guide to IMMUNOPHARMACOLOGY. N*ucleic Acids Research 46*: D1091–D1106.

Hogg, R.C., and Bertrand, D. (2007). Partial agonists as therapeutic agents at neuronal nicotinic acetylcholine receptors. *Biochemical Pharmacology 73*: 459–468.

Horenstein, N.A., Leonik, F.M., and Papke, R.L. (2008). Multiple Pharmacophores for the Selective Activation of Nicotinic α7-Type Acetylcholine Receptors. *Molecular Pharmacology 74*: 1496–1511.

Huang, S., Li, S.-X., Bren, N., Cheng, K., Gomoto, R., Chen, L., et al. (2013). Complex between α-bungarotoxin and an α7 nicotinic receptor ligand-binding domain chimaera. *Biochemical Journal 454*: 303–310.

Jha, A., Cadugan, D.J., Purohit, P., and Auerbach, A. (2007). Acetylcholine Receptor Gating at Extracellular Transmembrane Domain Interface: the Cys-Loop and M2–M3 Linker. *Journal of General Physiology 130*: 547–558.

Jorgensen, W.L., Chandrasekhar, J., Madura, J.D., Impey, R.W., and Klein, M.L. (1983). Comparison of simple potential functions for simulating liquid water. *Journal of Chemical Physics 79*: 926–935.

Kabsch, W., and Sander, C. (1983). Dictionary of protein secondary structure: Pattern recognition of hydrogen-bonded and geometrical features. *Biopolymers 22*: 2577–2637.

Khiroug, S.S., Harkness, P.C., Lamb, P.W., Sudweeks, S.N., Khiroug, L., Millar, N.S., et al. (2002). Rat nicotinic ACh receptor α7 and β2 subunits co-assemble to form functional heteromeric nicotinic receptor channels. *The Journal of Physiology 540*: 425–434.

Lee, W.Y., Free, C.R., and Sine, S.M. (2009). Binding to Gating Transduction in Nicotinic Receptors: Cys-Loop Energetically Couples to Pre-M1 and M2–M3 Regions. *Journal of Neroscience 29*: 3189–3199.

Lindorff-Larsen, K., Piana, S., Palmo, K., Maragakis, P., Klepeis, J.L., Dror, R.O., et al. (2010). Improved side-chain torsion potentials for the Amber ff99SB protein force field. Proteins: Structure, Function, and *Bioinformatics 78*: 1950–1958.

Marcovich, I., Moglie, M.J., Carpaneto Freixas, A.E., Trigila, A.P., Franchini, L.F., Plazas, P.V., et al. (2020). Distinct Evolutionary Trajectories of Neuronal and Hair Cell Nicotinic Acetylcholine Receptors. *Molecular Biology and Evolution 37*: 1070–1089.

Maskos, U., Molles, B.E., Pons, S., Besson, M., Guiard, B.P., Guilloux, J.-P., et al. (2005). Nicotine reinforcement and cognition restored by targeted expression of nicotinic receptors. *Nature 436*: 103–107.

McCormack, T.J., Melis, C., Colón, J., Gay, E.A., Mike, A., Karoly, R., et al. (2010). Rapid desensitisation of the rat α7 nAChR is facilitated by the presence of a proline residue in the outer β-sheet. *Journal of Physiology 588*: 4415–4429.

Meltzer, R.H., Thompson, E., Soman, K.V., Song, X.-Z., Ebalunode, J.O., Wensel, T.G., et al. (2006). Electrostatic Steering at Acetylcholine Binding Sites. *Biophysical Journal 91*: 1302–1314.

Morales-Perez, C.L., Noviello, C.M., and Hibbs, R.E. (2016). X-ray structure of the human α4β2 nicotinic receptor. *Nature 538*: 411–415.

Moroni, M., Vijayan, R., Carbone, A., Zwart, R., Biggin, P.C., and Bermudez, I. (2008). Non-Agonist-Binding Subunit Interfaces Confer Distinct Functional Signatures to the Alternate Stoichiometries of the α4β2 Nicotinic Receptor: An α4–α4 Interface Is Required for Zn^{2+} Potentiation. *Journal of Neuroscience 28*: 6884–6894.

Nielsen, B.E., Minguez, T., Bermudez, I., and Bouzat, C. (2018). Molecular function of the novel α7β2 nicotinic receptor. *Cell and Molecular Life Sciences 75*: 2457–2471.

Oliveira, A.S.F., Shoemark, D.K., Campello, H.R., Wonnacott, S., Gallagher, T., Sessions, R.B., et al. (2019). Identification of the Initial Steps in Signal Transduction in the α4β2 Nicotinic Receptor: Insights from Equilibrium and Nonequilibrium Simulations. *Structure 27*: 1171-1183.e3.

Purohit, P., and Auerbach, A. (2013). Loop C and the mechanism of acetylcholine receptor–channel gating. *Journal of General Physiology 141*: 467–478.

Puskar, N.L., Xiu, X., Lester, H.A., and Dougherty, D.A. (2011). Two Neuronal Nicotinic Acetylcholine Receptors, α4β4 and α7, Show Differential Agonist Binding Modes. *Journal of Biological Chemistry 286*: 14618–14627.

Rego-Campello, H., Del Villar, S.G., Honraedt, A., Minguez, T., Oliveira, A.S.F., Ranaghan, K.E., et al. (2018). Unlocking Nicotinic Selectivity via Direct C–H Functionalization of (−)-Cytisine. *Chem 4*: 1710–1725.

Revah, F., Bertrand, D., Galzi, J.-L., Devillers-Thiéry, A., Mulle, C., Hussy, N., et al. (1991). Mutations in the channel domain alter desensitisation of a neuronal nicotinic receptor. Nature *353*: 846–849.

Sokalingam, S., Raghunathan, G., Soundrarajan, N., and Lee, S.-G. (2012). A Study on the Effect of Surface Lysine to Arginine Mutagenesis on Protein Stability and Structure Using Green Fluorescent Protein. *PLOS ONE 7*: e40410.

Sousa da Silva, A.W., and Vranken, W.F. (2012). ACPYPE - AnteChamber PYthon Parser interfacE. *BMC Research Notes 5*: 367.

Tonstad, S., Davies, S., Flammer, M., Russ, C., and Hughes, J. (2010). Psychiatric Adverse Events in Randomized, Double-Blind, Placebo-Controlled Clinical Trials of Varenicline. *Drug-Safety 33*: 289–301.

Williams, D.K., Stokes, C., Horenstein, N.A., and Papke, R.L. (2009). Differential Regulation of Receptor Activation and Agonist Selectivity by Highly Conserved Tryptophans in the Nicotinic Acetylcholine Receptor Binding Site. *Journal of Pharmacology and Experimental Therapeutics 330*: 40–53.

Xiu, X., Hanek, A.P., Wang, J., Lester, H.A., and Dougherty, D.A. (2005). A Unified View of the Role of Electrostatic Interactions in Modulating the Gating of Cys Loop Receptors. *Journal of Biological Chemistry 280*: 41655–41666.

Yan, H., Pan, N., Xue, F., Zheng, Y., Li, C., Chang, Y., et al. (2015). The coupling interface and pore domain codetermine the single-channel activity of the α7 nicotinic receptor. *Neuropharmacology 95*: 448–458.

Zhang, J., Xue, F., Whiteaker, P., Li, C., Wu, W., Shen, B., et al. (2011). Desensitisation of α7 Nicotinic Receptor Is Governed by Coupling Strength Relative to Gate Tightness. *Journal of Biological Chemistry 286*: 25331–25340.

Figure Legends

Figure 1. A) Chemical structure of the agonists ACh, cytisine and 10-methylcytisine. **B)** Dynamical behavior of ACh, cytisine and 10-methylcytisine bound to one agonist site in the human $\alpha4\beta2$ and $\alpha7$ nAChR subtypes. Probability density maps (with a 0.00001 Å^{-3} contour) for the positively charged group of the agonists are depicted as a blue mesh. The structure used as the starting point for the simulations is shown in grey. Abbreviations: cytisine, Cyt and 10-methylcytisine, MeCyt.
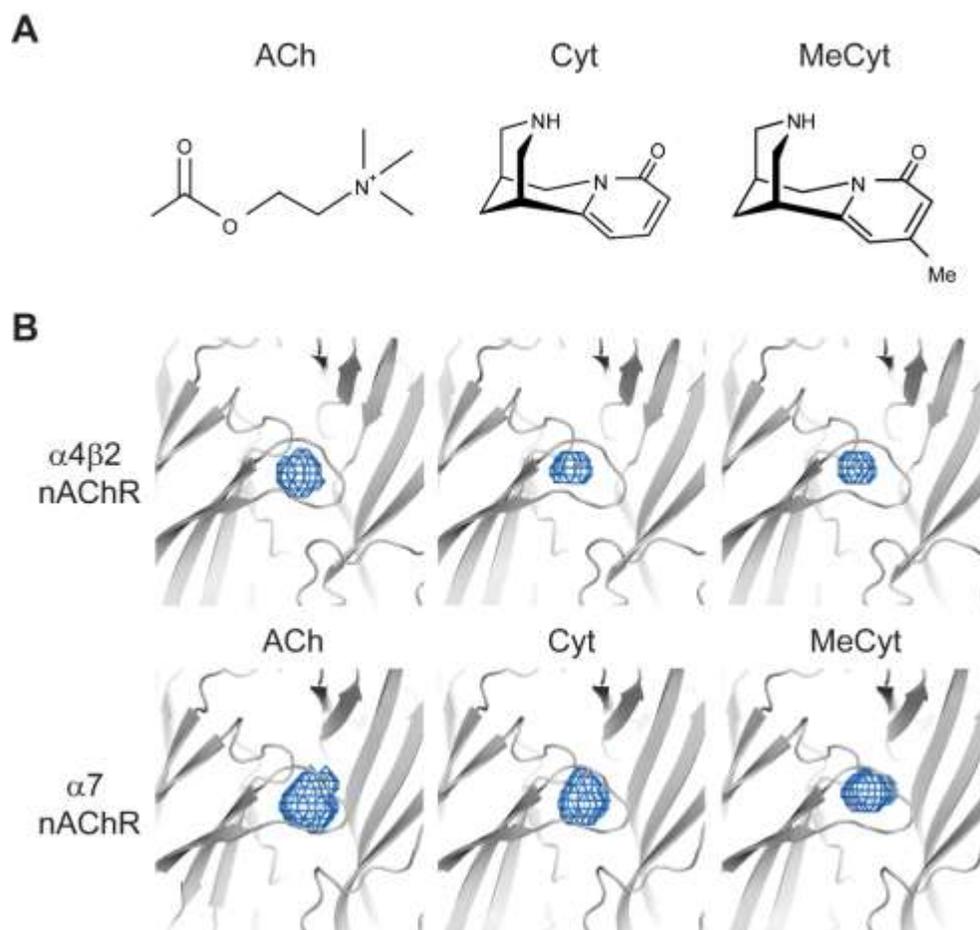
Figure 2. Dynamical behavior of the β3-strand arginine in **A)** α7 and **B)** α4β2 nAChR subtypes. Probability density maps for the arginine side chain are represented as a green mesh (contours at 0.00001 Å^{-3} for the Cζ). In the α7 nAChR, R101 is highly mobile, whereas in the α4β2 the equivalent residue (β2R106) mobility is reduced due to an interaction with α4D185 in loop B. The principal and complementary subunits are coloured in blue and orange, respectively. 10-Methylcytisine is represented in grey with sticks and spheres. In the α7 nAChR, R101 moves close to the methyl group at the C(10) position. **C)** Temporal evolution of the minimum distance between R101 (black line; left Y-axis) and TyrC1 (red line; right Y-axis) and 10-methylcytisine in the α7 nAChR. **D)** Temporal evolution of the minimum distance between R101 (black line; left Y-axis) and TyrC2 (red line; right Y-axis) and 10-methylcytisine in the α7 nAChR. Abbreviations: 10-methylcytisine, MeCyt.
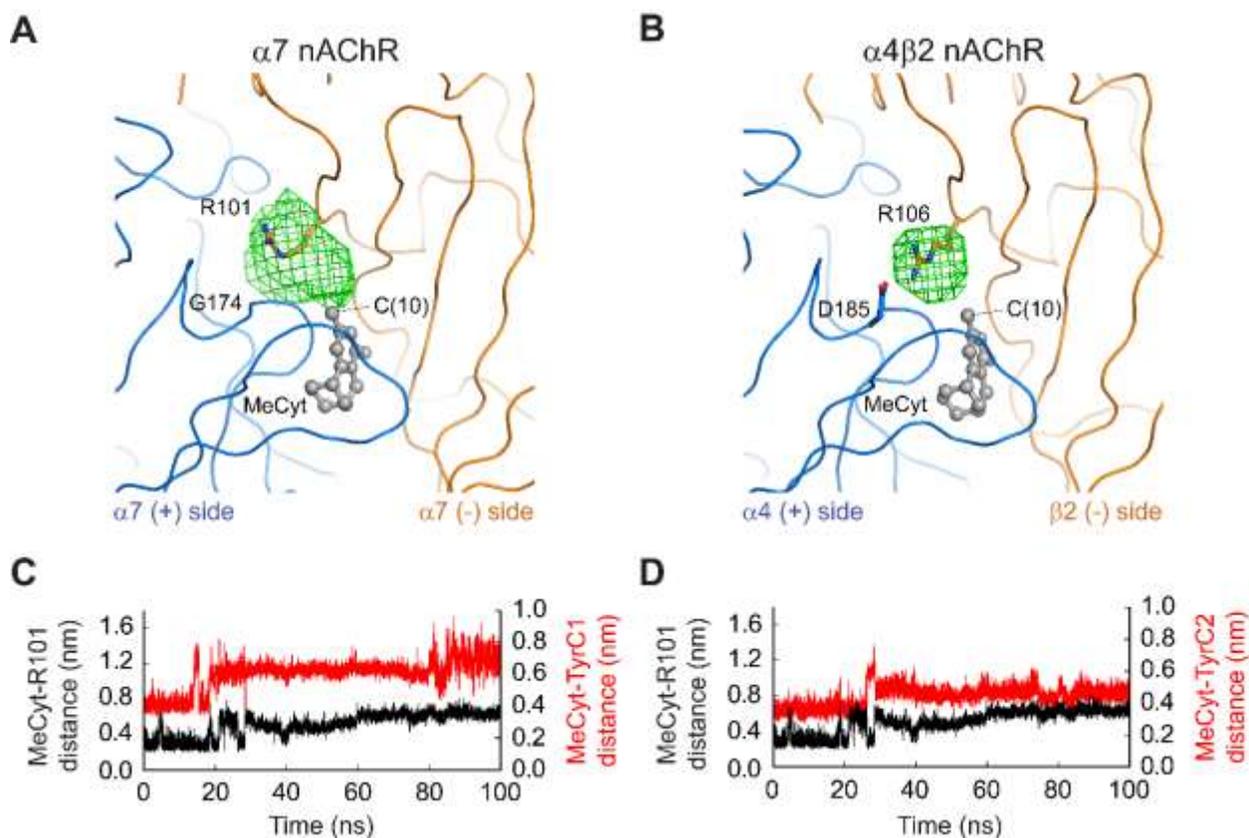
Figure 3. Overall distribution of the minimum distance between the sidechain of **A)** α7R101 and α7E215 in loop C and between β2R106 and **B)** α4D185 or **C)** α4E228. The histograms reflect the distances over the two nonconsecutive binding pockets of the receptors. Panels on the right show the position of the side chains of α7R101 and α7E215 and β2R106 and α4D185, α4D185 and α4E228 in the binding pockets. The principal subunit is shown in blue and the complementary in orange. The residues numbering refers to the following UniProt sequence codes: P43681 (α4 subunit), P17787 (β2 subunit) and P36544 (α7 subunit). Note that we include the signal peptide in the numbering. Abbreviations: cytisine, Cyt and 10-methylcytisine, MeCyt.
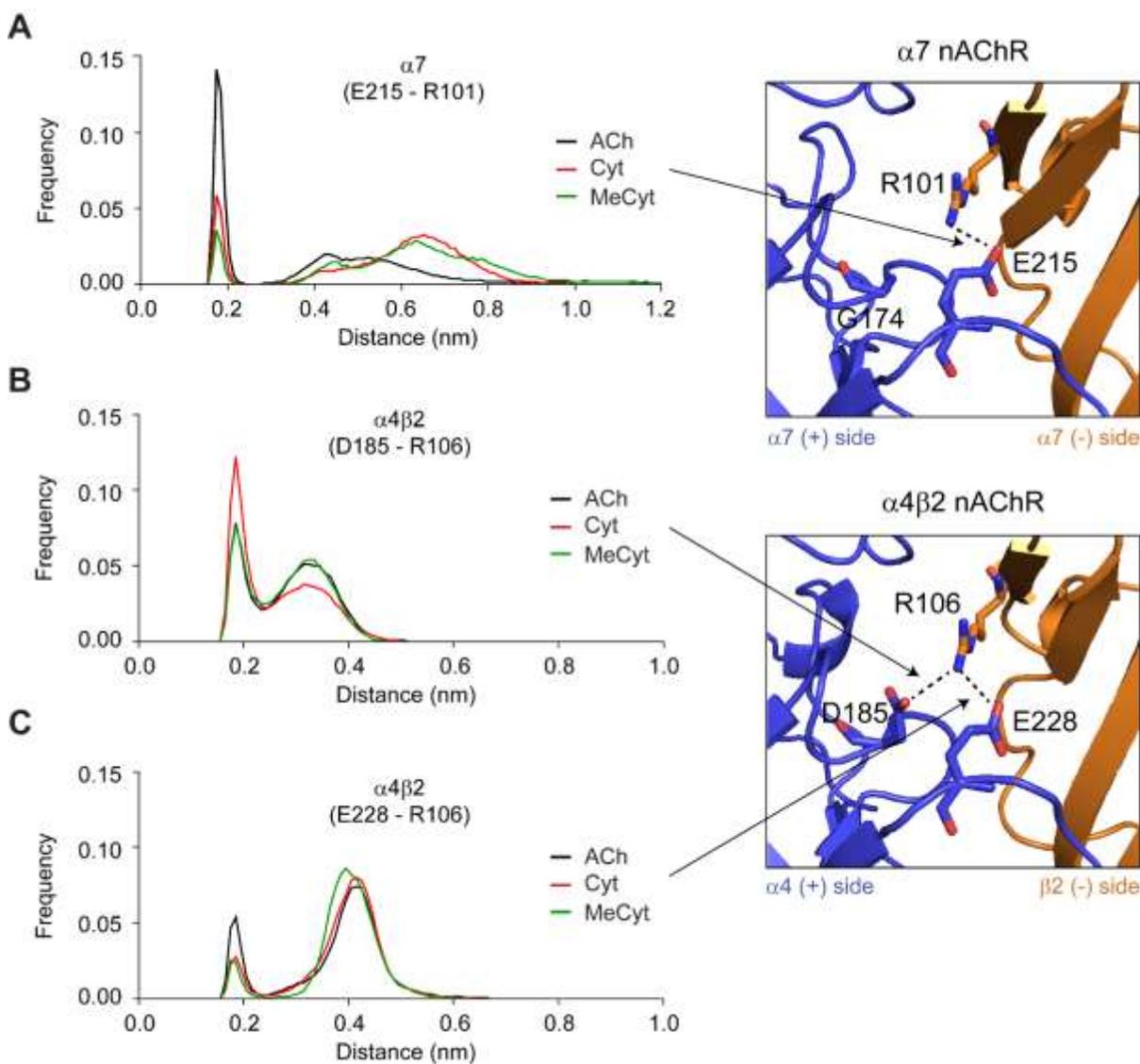
Figure 4. R101-D174 salt-bridge in MD simulations of α7G174D complexes. Overall distribution of the minimum distance between the sidechains of R101 (complementary subunit) and **A)** D174 (principal subunit) or **B)** E215 (principal subunit) in the α7G174D mutant receptor. The histograms reflect the distances over the two binding pockets bound to ACh (black line), cytisine (red line) and 10-methylcytisine (green line). Overall distribution of the distance between the charged N atom of cytisine and the sidechain of **C)** TyrA (α7I115) or **D)** TrpD (α7W77), two conserved aromatic residues lining the binding pockets in the α7 (black line) and α7G174D (orange line) systems. Panel on the right shows the position of D174, R101 and E215 in the cytisine-bound α7 complex. The principal subunit is shown in blue and the complementary in orange. Abbreviations: cytisine, Cyt; 10-methylcytisine, MeCyt.
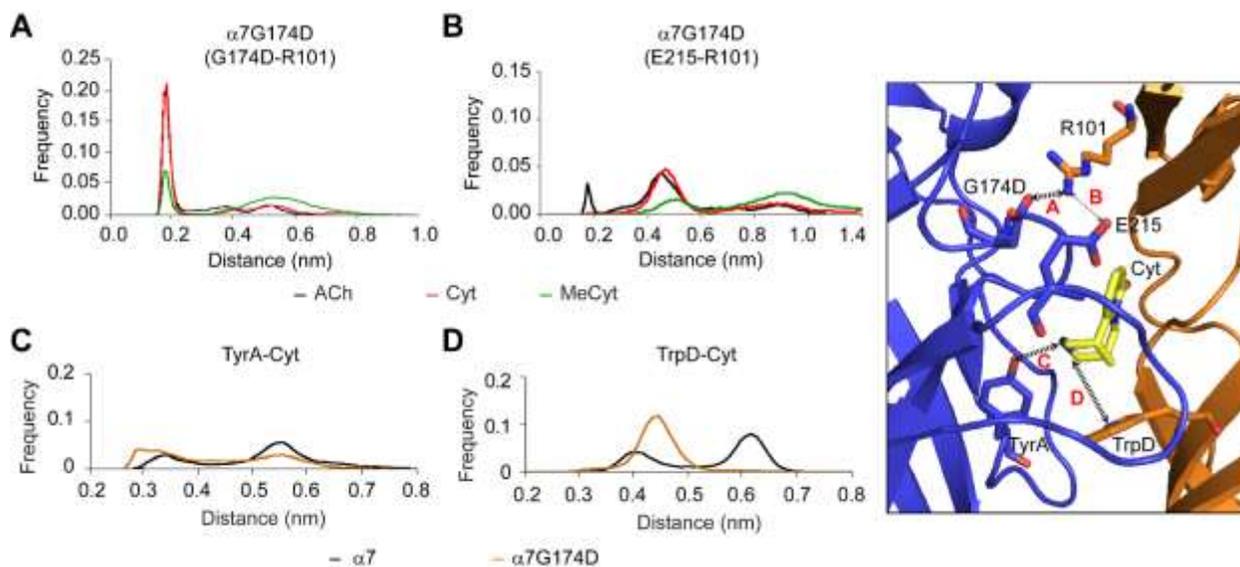
Figure 5. Functional effects of the R101-G174D salt-bridge. **A)** Agonist concentration-response curves for $\alpha 7$ (black line and circles) and $\alpha 7$G174D (red line and squares) receptors. **B)** Comparison of the concentration-response relationships of $\alpha 7$ (black circles and line) and $\alpha 7$G174D,R101K (yellow diamonds and line) and $\alpha 7$G174E,R101K (purple triangle and line). Data points in the concentration-response curves shown in A and B represent the mean ± SEM of 10-12 experiments carried out using 6-8 different *Xenopus* donors. Peak current amplitudes for all agonists were normalized to 1 mM, a maximally efficacious ACh concentration at the receptors for which we obtained full concentration-response curves. Estimated parameters EC_{50} and maximal relative efficacy (I_{Max}/I_{MaxACh}) are shown in Table 1. Abbreviations: cytisine, Cyt and 10-methylcytisine, MeCyt. **C)** Schematic representation of the minimum possible distance between the residues in positions 174 in loop B and 101 in β3-strand of the $\alpha 7$ nAChR.
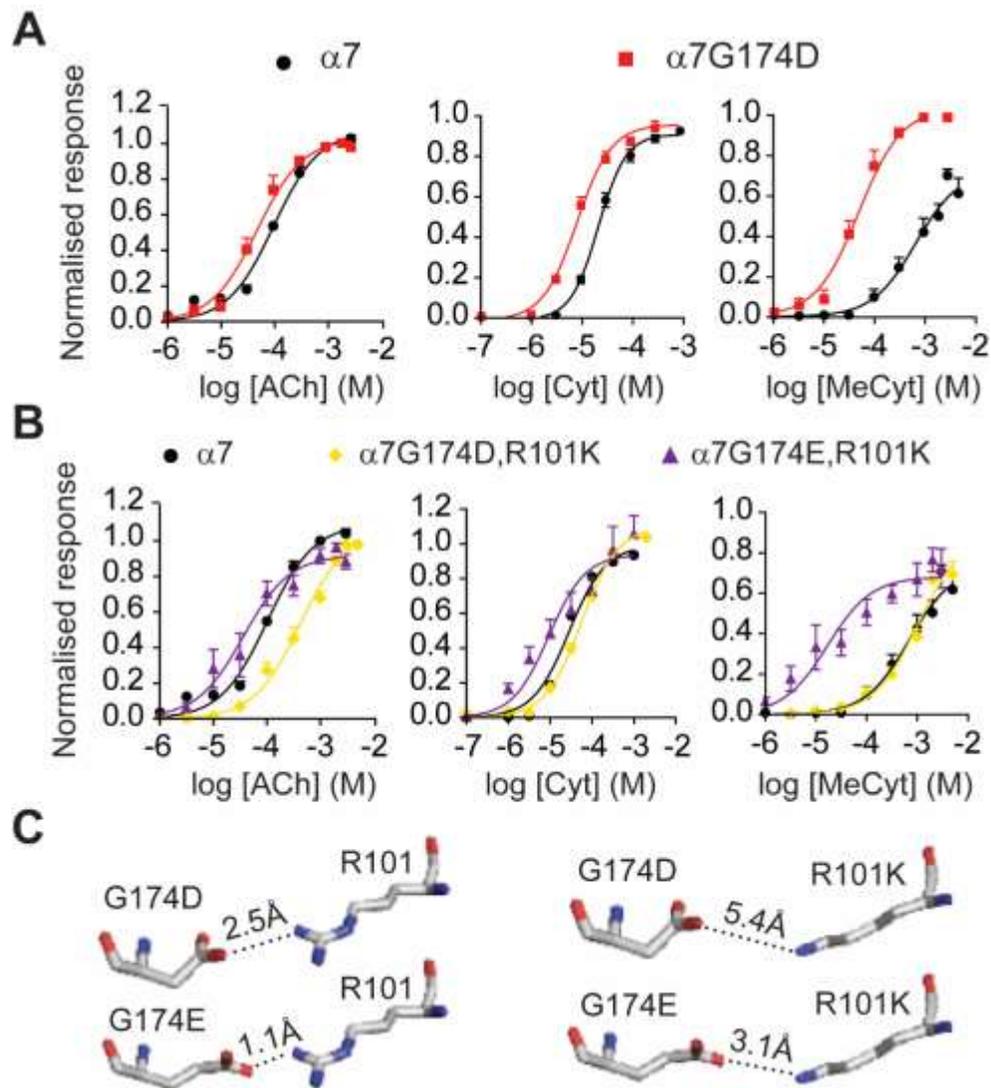
Figure 6. Comparison between single-channel profiles of α7 and α7G174D nAChR activated by ACh or cytisine. **A)** Typical traces of single-channel currents activated by ACh (top traces) or cytisine (bottom traces) in α7 and α7G174D receptors. Single-channel currents were measured using the cell-attached configuration on BOSC23 cells transiently expressing wild type α7 or α7G174D receptors. The single channel currents were elicited by approximately EC_{50} agonist concentrations at the receptors tested (ACh: 100 μM for α7 and α7G174D; cytisine: 25 μM cytisine for α7 and 10 μM for α7G174D). **B)** Scatter plots of the mean open (τ_{open}, black) and burst (τ_{burst}, grey) durations for α7 and α7G174D in the presence of ACh or cytisine at their EC_{50} concentrations. The estimated parameters are shown in Table S3. Data were obtained from single-channel recordings at a membrane potential of -70 mV. The open time corresponds to the longest component of the open time histogram. Burst durations were determined by the longest component of the burst histogram (see Figure S2). **C)** Representative inward current responses following the sustained application of ACh (1 mM, indicated by the horizontal bar) for oocytes expressing α7 or α7G174D receptors. For both receptor types, the onset of current decay was biphasic, and the fast (τf) and slow time (τs) constants of the decay were similar (α7: τf, 223 ± 77 ms, τs 1.4±0.4 s; α7G174D, τf 270 ± 50 ms, τs 0.9 ±0.2 s; n =10, N =6. Abbreviations: cytisine, Cyt.

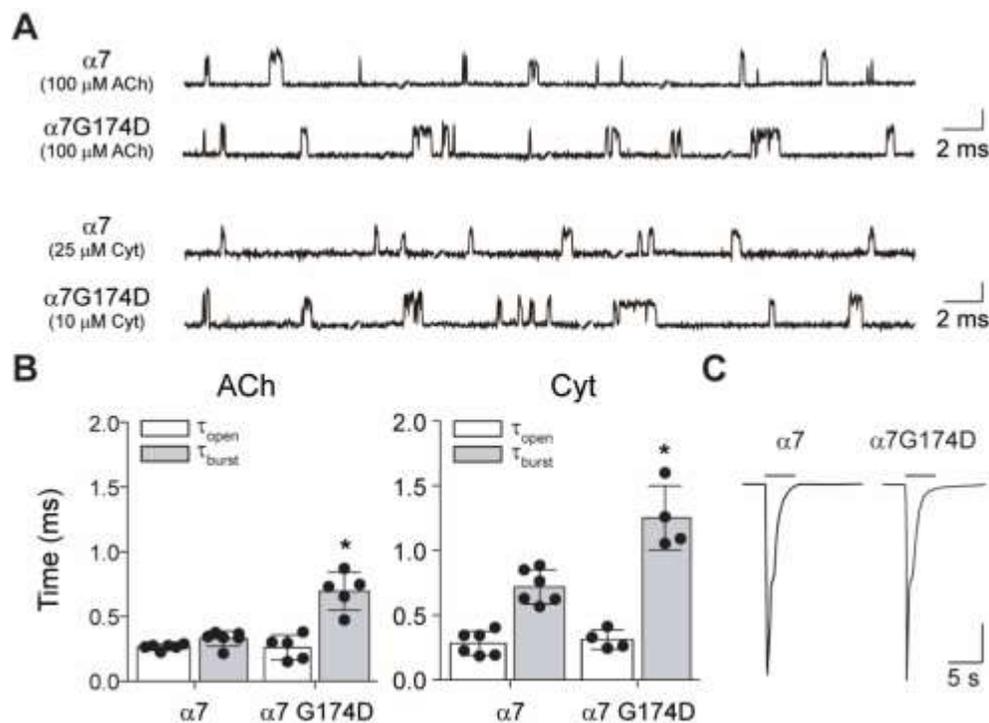**Figure 7.** Macroscopic and microscopic current responses of α7R101A nAChR to agonists. **A)** Agonist concentration-response curves for ACh, cytisine and 10-methylcytisine in α7 (black line and circles) or α7R101A (blue line and triangles) receptors. Data points represent 10-12 experiments carried out in 6 to 8 different batches of *Xenopus* oocytes. **B)** Single-channel currents of α7 or α7R101A activated by approximately EC_{50} concentrations of ACh (α7: 100 μM; α7R101A: 500 μM) or cytisine (α7: 25 μM α7R101A: 500 μM). Recordings were made in the cell-attached patch configuration at a membrane potential of -70 mV, as detailed in Methods. **C)** Typical traces of the macroscopic current elicited by saturating ACh concentrations of α7 (1 mM ACh) and α7R101A (3 mM ACh). The decay of the responses was biphasic and R101A drastically increased the fast and slow constants of decay: α7, τf 223 ± 77 ms and τs 1.4 ± 0.4 s vs α7R101A τf 1.01 ± 0.055 s and τs 2.7± 0.8 s; n =10; N = 6, p < 0.05). Abbreviations: cytisine, Cyt and 10-methylcytisine, MeCyt.
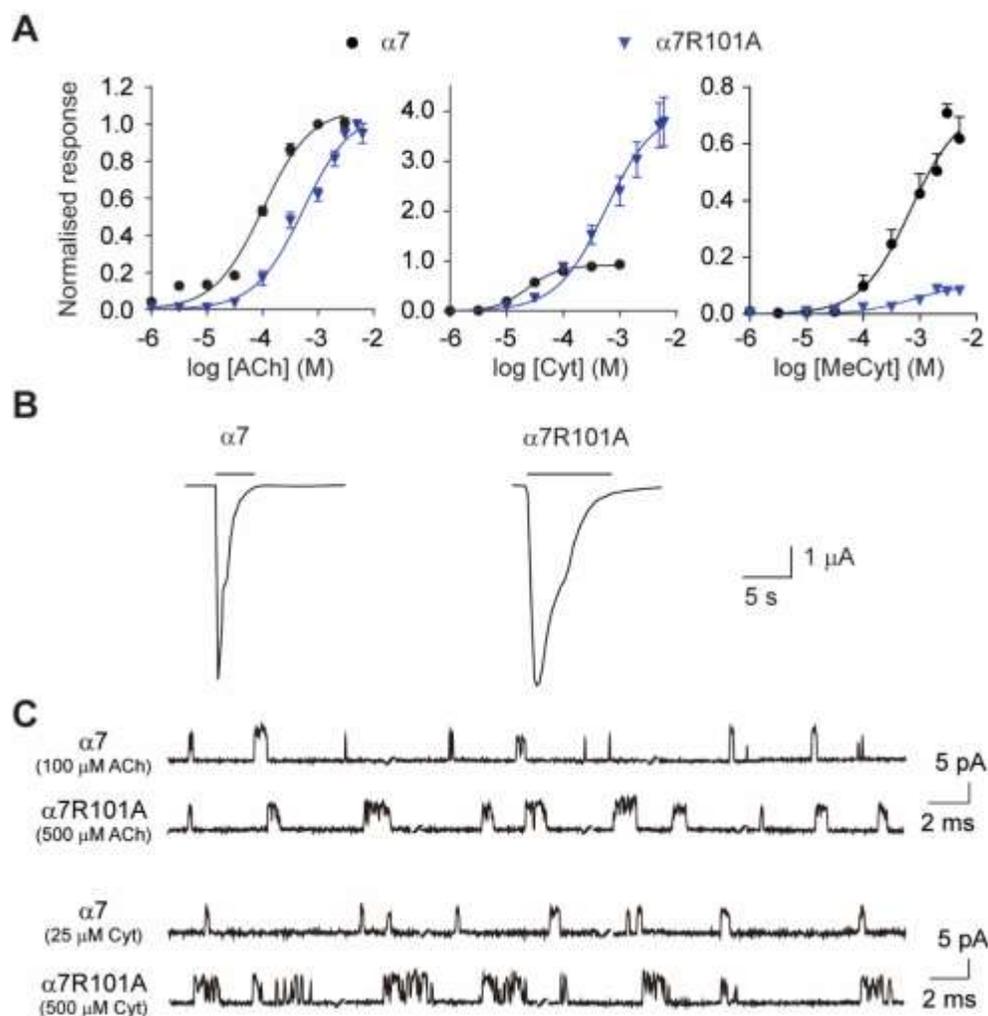
Figure 8. Average RMSF difference between α7 and α7R101A systems. **A)** Average change in Cα RMSF between the α7 and α7R101A systems with ACh (black line) cytisine (red line) or 10-methylcytisine (green line) bound in one of the two nonconsecutive binding pockets of the receptor. The RMSF differences for the principal (left side image) and complementary (right side image) subunits are shown. See SI Figure S11 to for the corresponding data obtained from the second binding pocket. **B)** Average RMSF difference between α7 and α7R101A systems bound to ACh, cytisine or 10-methylcytisine mapped into the average structure of each system. The structure colours are related to the average RMSF difference: the red and blue regions correspond to the residues with the largest differences between the two systems. Abbreviations: cytisine, Cyt and 10-methylcytisine, MeCyt.
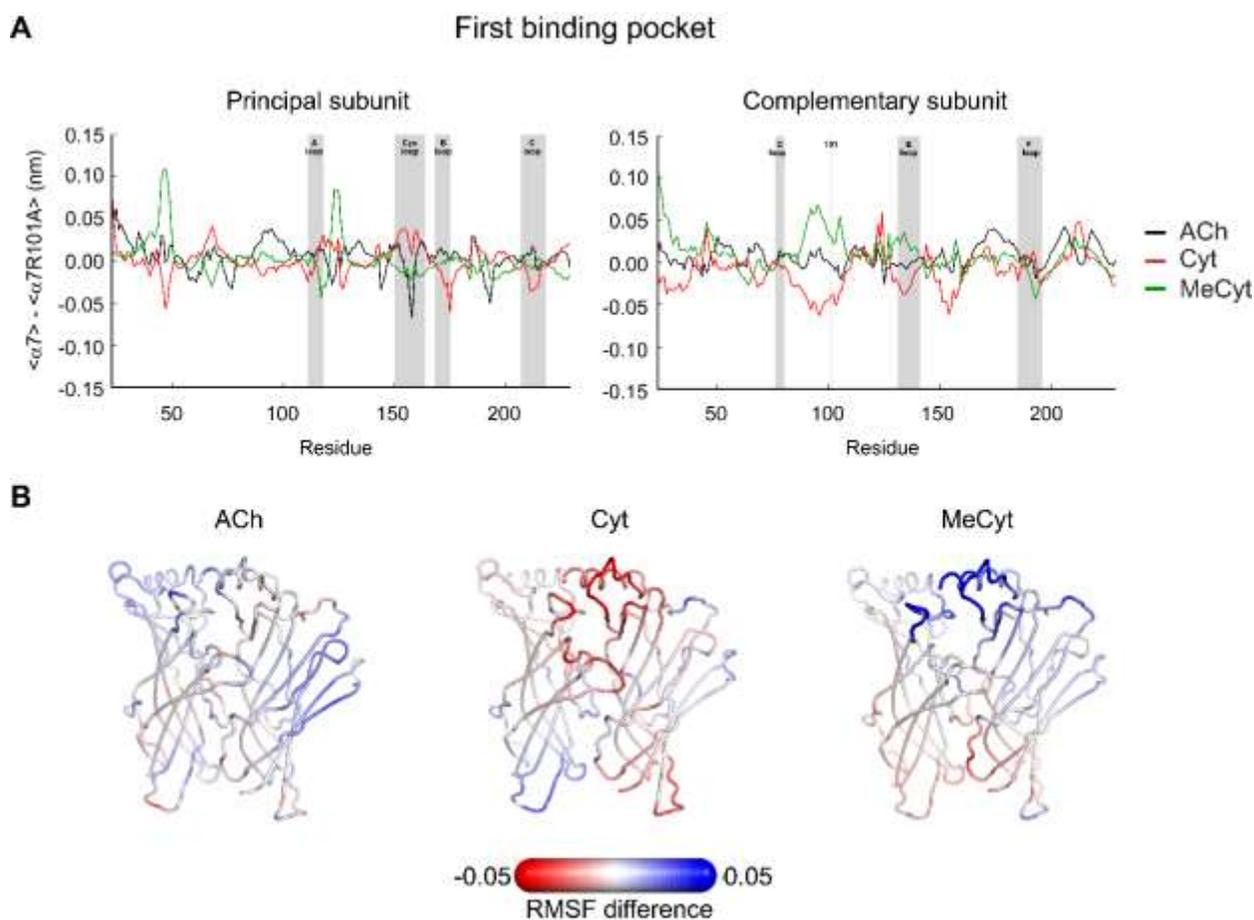
Figure 9. Average structure of agonist-bound α7 and α7R101A complexes. The agonist simulated were **A)** ACh, **B)** cytisine and **C)** 10-methylcytisine bound in one of the two nonconsecutive binding pockets of the receptor. Note that for the cytisine-bound α7 complex (shown in blue), there is a clear change in the extent of loop C capping, compared to the α7R101A complex (shown in grey). The structures shown here represent the average structure calculated over all replicates for each system, as described in Methods. Abbreviations: cytisine, Cyt and 10-methylcytisine, MeCyt.
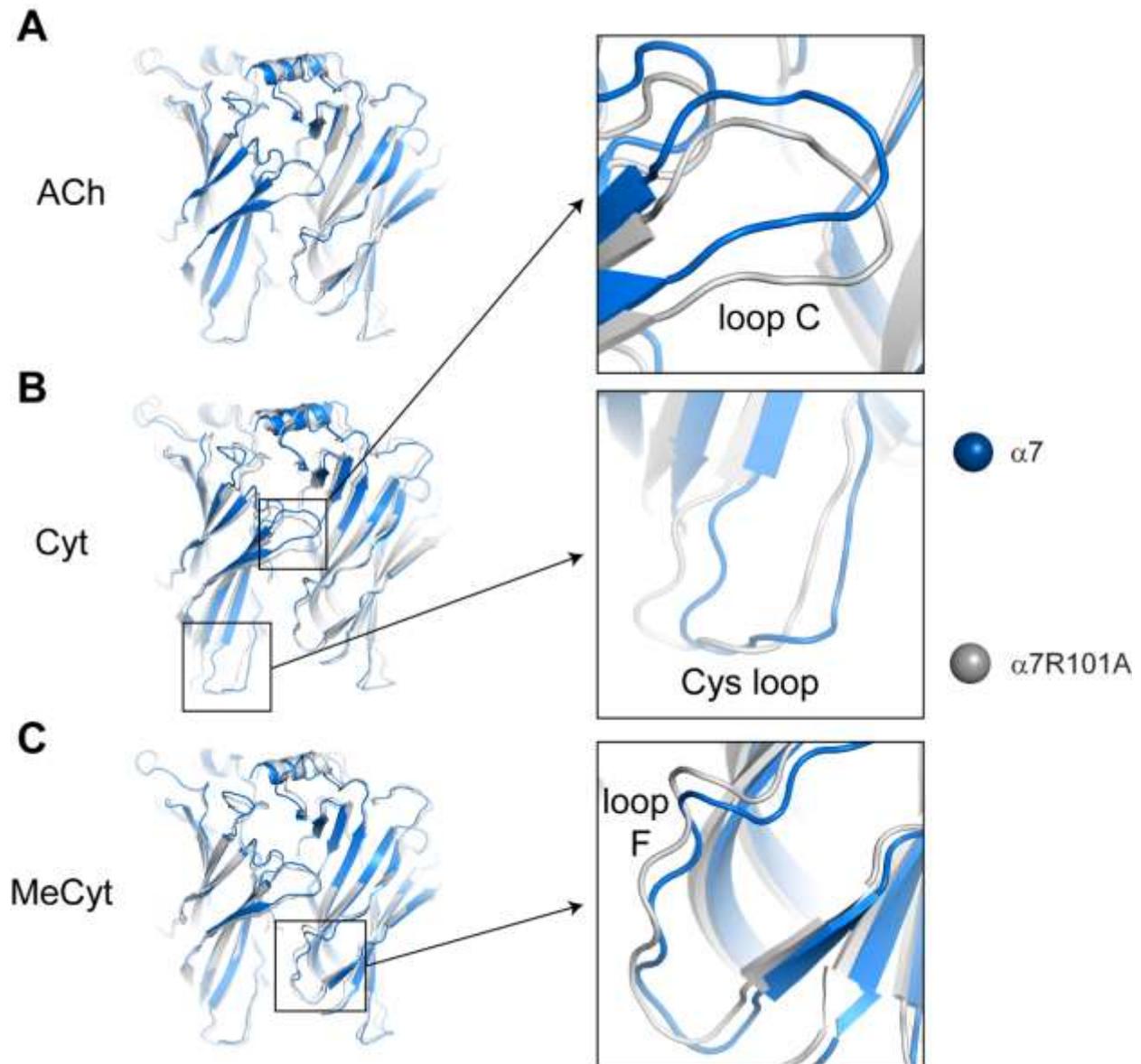
Table 1. R101 of β3-strand influences agonist potency and efficacy in the α7 nAChR subtype.

Mutation	ACh		Cytisine		10-Methylcytisine	
	EC_{50} (μM) (95% CI)	I_{max}/I_{AChMax} (95% CI)	EC_{50} (μM) (95% CI)	I_{max}/I_{AChMax} (95% CI)	EC_{50} (μM) (95% CI)	I_{max}/I_{AChMax} (95% CI)
α7	82.4 (71-95)	1	28 (22-36)	0.93 (0.90-0.94)	643 (493-837)	0.55 (0.4-0.7)
α7G174D	66.9 (37-120)	1	8.5* (5.4-7.4)	0.95 (0.8-1.1)	139.6* (100-190)	0.92* (0.8-1.0)
α7G174A	86 (38-194)	1	60.11 (19-191)	1.40 (1.0-1.8)	891 (545-1459)	0.40 (0.2-0.6)
α7G174E	322 * (181-568)	1	273* (161-463)	1.17 (0.8-1.5)	1025.6* (120-8749)	0.75 (0.5-0.9)
α7R101A	540* (398-794)	1	389* (299-504)	4.10* (2.4-6.0)	2075* 440-7943	0.39 (0.06-0.85)
α7R101D	ND	ND	ND	ND	ND	ND
α7R101D, G174R	ND	ND	ND	ND	ND	ND
α7R101K	741* (506-1086)	1	122* (63-236)	1.05 (0.8-1.3)	3228* (2523-4130)	0.56 (0.2-0.9)
α7G174D, R101K	349* (222-550)	1	54 (25-112)	1.26 (1.1-1.5)	1303 (902-1888)	0.96* (0.7-1.2)
α7G174E, R101K	54 (36-79)	1	7.81* (3-20)	1.04 (0.8-1.3)	69.34* (36-132)	0.68 (0.5-0.8)
α7E215A	148* (83-260)	1	85.9* (52-140)	1.12 (1.0-1.3)	1140* (756-1713)	0.95 (0.6-1.2)

EC_{50} and normalised maximal current responses (relative efficacy) (I_{Max}/I_{AChMax}) were estimated as described in Methods. Data shown represent the mean +/- 95% confidence interval (CI) of n= 10-12 experiments carried out in 6 to 8 different batches of *Xenopus* oocytes. Statistical differences between wild type and mutant α7 receptors were determined by One Way Anova followed by Dunnett's or Bonbeforri's post hoc. *, denotes statistical difference ($p < 0.05$). ND, not determined due to low levels of functional expression: amplitude of the responses activated by 1, 3 or 5 mM of ACh were no greater than 90 nA. For example, the mean average for the current responses to 5 mM were 68 (55–80) nA for α7R101D receptors and 58 (48-70) nA for α7G174R,R101D (mean, 95 % CI; n = 15, N = 6).